Autonomous Navigation of a Formation of Spacecraft in the Proximity of a Binary Asteroid

By Francesco TORRE,[1)] Massimiliano VASILE,[1)] and Romain SERRA[1)]and Stuart GREY[1)]

[1)]*Department of Mechanical and Aerospace Engineering, University of Strathclyde, Glasgow, United Kingdom*

(Received June 21st, 2017)

The paper presents a study on the navigation of a formation of spacecraft in the proximity of a binary asteroid. A specific scenario is considered in which the spacecraft are orbiting at one of the triangular libration points under the assumption of a quasi circular orbit of the secondary with respect to the primary. This work investigates the use of an Unscented H_{infty} Filter and a data sharing mechanisms among spacecraft, plus the use of a novel polynomial algebra to replace the Unscented Transformation. The paper will show that the spacecraft can be maintained at the desired location using a combination of optical and LIDAR measurements shared across the formation.

Key Words: binary asteroids, formation flying, autonomous navigation

1. Introduction

Binary asteroids are systems composed of two asteroids orbiting around their common barycentre. Some of them are part of the Near Earth Object population, like 2000 DP107, or 65803 Didymos (1996 GT),an Apollo asteroid discovered on April 11, 1996, that is the target of the AIDA mission. Navigating in the proximity of an asteroid is in itself a challenging task due to the complex dynamics induced by the irregular gravity field of the asteroid, the gravity of the Sun and solar radiation pressure. Even more challenging is to navigate a formation of spacecraft with heterogeneous sensors. Recent work by one of the authors demonstrated the possibility to autonomously navigate a formation of spacecraft with a distributed fault-tolerant autonomous system[1)] . The complexity increases even further in the case of a binary due the interaction between the primary and the secondary.

This work extends, to the case of a binary system, previous results on the navigation of single spacecraft and of a formation of spacecraft in the proximity of an asteroid[1),2)] The paper will focus, in particular, on the maintenance of a subset of periodic solutions that can be of particular interest for the exploration of a binary system or to conduct deflection and prospection experiments (see Fig. 1). Periodic solutions around the dynamic equivalent of the Lagrange points L4 and L5 of the binary system were shown to be of particular interest to extract surface and subsurface material with laser ablation[3)] . The dynamical model in the proximity of the binary system includes the gravity of the two asteroids, the gravity of the Sun and solar radiation pressure. Each spacecraft is equipped with a minimum set of sensors under the assumption of low power and low computational capabilities. Following previous work from the authors each spacecraft is assumed to carry a laser range finder, a camera and an inter satellite link that allows sharing information with other spacecraft in the formation and provides range and range rate information.

Two scenarios will be considered in this study: one in which one single spacecraft combines telemetry from Earth with local measurements, the other in which a formation of spacecraft autonomously navigate with no measurement from Earth. It will be shown that the combination of camera and laser range finder substantially improves the navigation accuracy and that the intersatellite link allows the formation to autonomously navigate and control their position near L4. Given the nonlinear nature of the dynamics the paper will propose the use of a generalised polynomial algebra[4)] to propagate the uncertainty region. The algebra replaces the Unscented Transformation in the Unscented H-infinity Filter.

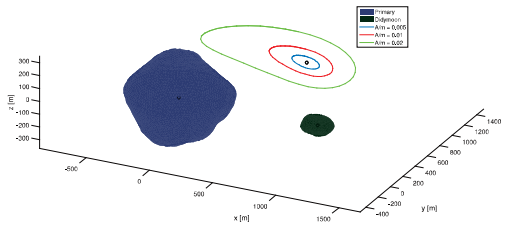

Fig. 1. Periodic orbits at L4 in the asteroid binary system.

The paper starts with the description of the dynamics and the measurement model, it will then present the state estimation and data fusion strategy, including the use of the new algebra. Some results and conclusions will complete the paper.

2. Dynamic Model

The reference frame chosen for the simulation of the dynamical system and the navigation of the formation of spacecraft is a non-rotating reference frame, centered in the centre of mass of the binary asteroid system (see Fig. 2). In such a frame, it is assumed that the motion of the asteroids is known and consisting of circular coplanar orbits with rotation period equal to the rotation period of the system. Both the asteroids can rotate around their respective rotation axes according to literature. The further assumption is that, while the primary asteroid is considered to

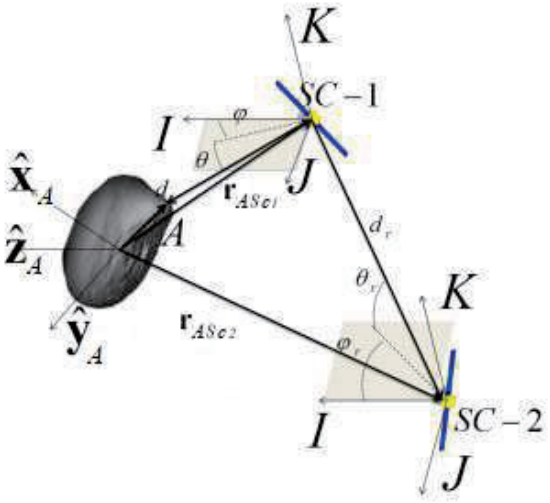

Fig. 2. Reference frame for dynamics and measurement model.

be a homogeneous sphere, the secondary is a homogeneous ellipsoid with semi-axes a_B , b_B and c_B, rotating around the z-axis with angular velocity ω_B[5] .

The gravity field of the secondary asteroid can be expressed as the sum of a spherical field plus a second-degree and second-order field:[6]

$$U_{20,22} = \frac{\mu_B}{\delta r_{BSc_i}^3}\left[C_{20}\left(1-\frac{3}{2}\cos^2(\theta_B)\right) + 3C_{22}\cos^2(\theta_B)\cos(2\varphi_B)\right] \quad (1)$$

where δr_{BSc_i} is the relative position vector between the asteroid B and the spacecraft i in the body-fixed frame B, μ_B is the asteroid gravitational constant, the harmonic coefficients C_{20} and C_{22} are a function of the semi-axes:

$$\begin{aligned} C_{20} &= -\frac{1}{10}\left(2{c_B}^2 - {a_B}^2 - {b_B}^2\right) \\ C_{22} &= \frac{1}{20}\left({a_B}^2 - {b_B}^2\right) \end{aligned} \quad (2)$$

and θ_B and φ_B are the longitude and latitude angles respectively:

$$\theta_B = \tan^{-1}\left(\frac{z_B}{\sqrt{{x_B}^2+{y_B}^2}}\right);\ \varphi_B = \tan^{-1}\left(\frac{y_B}{x_B}\right) \quad (3)$$

The conversion from the body-fixed frame to the reference one is obtained by the simple rotation matrix:

$${}^{I}R_B = \begin{pmatrix} \cos(\omega_B t) & -\sin(\omega_B t) & 0 \\ \sin(\omega_B t) & \cos(\omega_B t) & 0 \\ 0 & 0 & 1 \end{pmatrix} \quad (4)$$

where t indicates the time. The spacecraft is assumed to be subject to the gravitational force of the Sun, solar radiation pressure and the irregular gravity of the binary system. Being $\mathbf{r}_A$ the position of asteroid A, $\mathbf{r}_B$ the one of asteroid B, $\mathbf{r}_S$ the one of the Sun and $\mathbf{r}_{Sc_i}$ the one of the i-th spacecraft all in the chosen reference frame, defining $\mathbf{r}_{ASc_i} = \mathbf{r}_{Sc_i} - \mathbf{r}_A$, $\mathbf{r}_{BSc_i} = \mathbf{r}_{Sc_i} - \mathbf{r}_B$ and $\mathbf{r}_{SSc_i} = \mathbf{r}_{Sc_i} - \mathbf{r}_S$ as the relative position vectors from the i-th spacecraft to the asteroids A and B and the Sun respectively, the nonlinear equations of motion are:

$$\begin{aligned} \ddot{\mathbf{r}}_{Sc_i} = & -\frac{\mu_A}{\|\mathbf{r}_{ASc_i}\|^3}\mathbf{r}_{ASc_i} \\ & -\left[\frac{\mu_B}{\|\mathbf{r}_{BSc_i}\|^3} + {}^{I}R_B\left(\frac{\partial U_{20,22}}{\partial \delta r_{BSc_i}}\right)_B\right]\mathbf{r}_{BSc_i} \\ & -\frac{\mu_S}{\|\mathbf{r}_{SSc_i}\|^3}\mathbf{r}_{SSc_i} + \frac{\mu_S}{\|\mathbf{r}_S\|^3}\mathbf{r}_S + \mathbf{a}_{SRP} + \mathbf{u} \end{aligned} \quad (5)$$

with μ_S, μ_A and μ_B being gravity constants of the Sun, asteroid A and B respectively. The quantity $\mathbf{a}_{SRP}$ represents the solar radiation pressure, defined as:

$$\mathbf{a}_{SRP} = C_{R_i} S_{SRP}\left(\frac{r_{1AU}}{r_{SSc_i}}\right)^2 \frac{A_i}{m_{Sc_i}}\hat{r}_{SSc_i} \quad (6)$$

where r_{SSc_i} is the distance of the i-th spacecraft from the Sun, A_i and m_{Sc_i} are the spacecraft cross sectional area and mass respectively, C_{R_i} is the reflectivity coefficient, S_{SRP} is the solar radiation pressure at 1 AU and r_{1AU} is one astronomical unit in km. The vector $\mathbf{u} = \left[u_x, u_y, u_z\right]^T$ in equation (5) is a control input, which will be defined later in Section **4.**.

If one considers a formation of 4 spacecraft, the vector equation (5) can be applied to each spacecraft independently and can be re-written in compact form as a system of first order differential equations:

$$\dot{\mathbf{X}} = f(\mathbf{X}, \mathbf{u}) \quad (7)$$

where $\mathbf{X} = [\mathbf{r}_{Sc_1}, \dot{\mathbf{r}}_{Sc_1}, \mathbf{r}_{Sc_2}, \dot{\mathbf{r}}_{Sc_2}, \mathbf{r}_{Sc_3}, \dot{\mathbf{r}}_{Sc_3}, \mathbf{r}_{Sc_4}, \dot{\mathbf{r}}_{Sc_4}]^T$ is the state vector containing the position and velocity of all the spacecraft.

3. Measurement Model

With reference to Figure 2, it is assumed that each spacecraft is provided with the following set of sensors and measurements:

- A camera which provides elevation and azimuth angles of centroid of the asteroid;
- A laser range finder which measures the distance from the spacecraft to a point on the asteroids surface;
- Inter-spacecraft measurements, which include the relative distance vector between two spacecraft, in terms of range, azimuth and elevation.

In the case of single spacecraft orbiting the system, the inter-spacecraft measurements are substituted by relative range, azimuth and elevation measurements obtained from a ground station. Note that in this paper we do not consider standard deep space navigation and tracking methods using, for example, DOR or Δ-DOR. These more realistic measurements will be introduced in future work.

3.1. Camera Model

In order to develop the measurement model of the camera, two intermediate reference frames are required as shown in Figure 3:

- Spacecraft coordinate system SC $\{x_{sc}\, y_{sc}\, z_{sc}\}$: the origin of this frame lies on the centre of mass of the spacecraft, with

the three symmetrical body axes defined as three coordinate axes[7] .

- Camera coordinate system C $\{\hat{x}_C\, \hat{y}_C\, \hat{z}_C\}$: the centre C is the perspective projection of the camera, with the z_C-axis parallel to the optical axis of the camera and directed to the centre of the asteroid. The image plane is defined as O_C-x_C y_C.

In this paper, it is assumed that the body reference frame of each spacecraft is aligned with the camera and the attitude is known with a level of precision corresponding to the one of the star tracker.

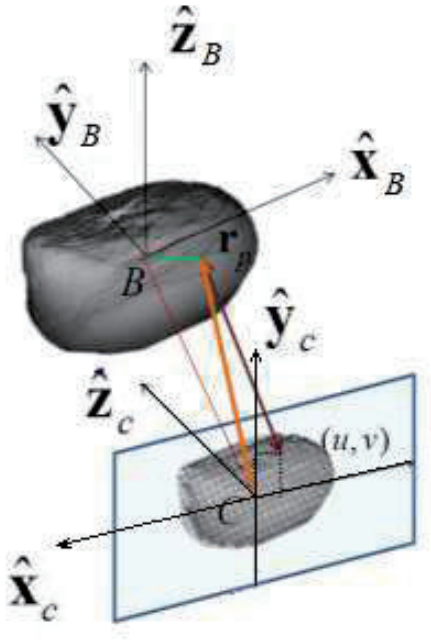

Fig. 3. Pin-Hole camera model.

A picture is generated by a graphics library according to the state of the system. Then, an ellipse fitting algorithm is used to compute the coordinates of the centroid of the asteroid in camera coordinates. Once the position of the centroid is known, the pointing angles can be computed by:

$$\varphi_C = \tan^{-1}\left(\frac{x_C}{f}\right);\ \psi_C = \tan^{-1}\left(\frac{y_C}{f/\cos(\varphi_C)}\right) \tag{8}$$

where f is the focal length of the camera. To these angles those required to go from the camera frame to the spacecraft frame are added. The model for the observation equations used in the filter, neglecting the contribution given by the attitude system, is:

$$\mathbf{z}_{camera} = \begin{bmatrix}\varphi\\ \psi\end{bmatrix} + \begin{bmatrix}\zeta_\varphi\\ \zeta_\psi\end{bmatrix} \tag{9}$$

where $\zeta_{\phi,\psi}$ comprise all the errors from attitude and centroiding process. Note that here the illumination conditions are not considered, so it is assumed that each spacecraft sees the whole visible surface from its position. This is is reasonable if one assumes that a complementary map could be built while starting the orbit acquisition, combining pictures from the whole formation.

3.2. Laser ranging Model

In general, the laser provides range from the spacecraft to a point on the surface of target object and works at a range from 50 m to 50 km.[8] It is assumed that the laser illuminates the point on the surface that corresponds to the centroid derived from the elaboration of the images acquired by the camera.[9] This distance is simply given by:

$$l = \|\mathbf{r}_{sc} - \mathbf{r}_{surf}\| \tag{10}$$

where $\mathbf{r}_{surf}$ is the position of a point on the asteroids surface along the centroid direction. The observation equation of the laser including the measurement noise is:

$$y_l = h_l(\mathbf{r}_{sc}) + \zeta_l = l + \zeta_l \tag{11}$$

with ζ_l the measurement noise. The accuracy of this measurement depends on the characteristic error of the sensor, along with a bias defined by the mounting error of the instrument. If the range l is pre-processed in combination with the angular measurements from equation (8), a relative position vector from the spacecraft to the point on the surface can be constructed as

$$\mathbf{z} = \begin{bmatrix}l\\ \varphi\\ \psi\end{bmatrix} = h(\mathbf{r}_{sc}) + \zeta \tag{12}$$

where z is the measurement vector obtained from the combination of camera and laser, $h(\mathbf{r}_{sc})$ is the vector containing the measurement model and ζ is the total measurement noise vector.

3.3. Inter-spacecraft Measurements

The set of inter-spacecraft measurements is represented by the relative position vector between two spacecraft in the formation. Similarly to the model in Section **3.2.**, this is composed of the relative distance, local azimuth and elevation.[10] The observation equation is given by:

$$\mathbf{z}_r = h_r\left(\mathbf{r}_{Sc_i},\ \mathbf{r}_{Sc_j}\right) = [d_r\ \varphi_r\ \psi_r]^T + \zeta_r \tag{13}$$

where $\zeta_r = \left[\zeta_{d_r}\ \zeta_{\varphi_r}\ \zeta_{\psi_r}\right]^T$ is the measurement noise.

3.4. Ground Station Measurements

The set of measurements defined by range ρ, azimuth φ and elevation ψ with respect to the ground station is used to estimate a spacecraft trajectory from Earth. These values are described in the East-North-Zenith reference frame:

$$\begin{aligned}\rho_{GS} &= \|\rho_{ENZ}\|\\ \varphi_{GS} &= \tan^{-1}\left(\frac{x_{ENZ}}{y_{ENZ}}\right)\\ \psi_{GS} &= \sin^{-1}\left(\frac{z_{ENZ}}{\rho}\right)\end{aligned} \tag{14}$$

where $\rho_{\mathbf{ENZ}} = [x_{ENZ}\ y_{ENZ}\ z_{ENZ}]^T$ is the position vector of the spacecraft measured from ground station. The value of the azimuth is computed Eastwards from the North direction. The observation equation is given as:

$$\mathbf{z}_{GS} = h_{GS}\left(\mathbf{r}_{Sc_i},\ \mathbf{r}_{GS}\right) + \zeta_{GS} = [\rho_{GS}\ \varphi_{GS}\ \psi_{GS}]^T + \zeta_{GS} \tag{15}$$

with ζ_{GS} assumed to be the measurement noise.

4. Control strategy

The control strategy aims at keeping each spacecraft orbiting on a trajectory proximal to the nominal one. Note that this is not an optimal control strategy but it is sufficient to demonstrate the effect of the navigation and data fusion algorithms. The control law is given by the simple PD controller:

$$\mathbf{u} = K_P\left(\begin{bmatrix}x\\y\\z\end{bmatrix}_G - \begin{bmatrix}x\\y\\z\end{bmatrix}_N\right) + K_D\left(\begin{bmatrix}\dot{x}\\\dot{y}\\\dot{z}\end{bmatrix}_G - \begin{bmatrix}\dot{x}\\\dot{y}\\\dot{z}\end{bmatrix}_N\right) \tag{16}$$

where the subscripts G and N stand for guidance and navigation respectively, K_P is the proportional coefficient and K_D is the derivative one. If the actual trajectory of the spacecraft is known, the continuous control in Eq. (16) can be introduced into the full dynamic model in Eq. (5). Here however, the trajectory is estimated by the navigation system with the actual position of the spacecraft never known exactly. The predicted estimation is used by the controller to maintain the relative formation (shown later in Section 5). Once the controller is inserted in the spacecraft dynamic model, one obtains a closed loop problem in which the control is performed together with the estimation, and the filter equations incorporate the action of the controller. During the controlled phases, it is assumed that the asteroid trajectory is precisely known; the state variables to be estimated are only those related to the spacecraft in the formation.

5. State Estimation and Data Fusion Strategy

The state estimation process is based on the same Uscented H_∞ Filter proposed in.[1)]

The UHF works on the premise that one can find a good approximation for the *a posteriori* covariance by propagating a limited set of optimally chosen samples.[11)] Using the estimation theory formalism, the nonlinear process in Eq. (7) and measurement equations in Section **3.** can be discretised in time and written as:

$$\begin{aligned}\mathbf{x}_{k+1} &= f(\mathbf{x}_k,\ \mathbf{u}_k)\\ \mathbf{y}_k &= h(\mathbf{x}_k,\ \mathbf{v}_k)\end{aligned} \tag{17}$$

where $\mathbf{v}_k$ is the measurement noise. The initial conditions are the estimated position and velocity from the filter at time t_k. The UHF relies on the unscented transformation to propagate a set of suitable sigma points, drawn from the *a priori* covariance matrix. The set of sigma points χ are given as:

$$\chi_i = \begin{cases}\tilde{\mathbf{x}}_k & i = 0\\ \tilde{\mathbf{x}}_k + \left(\sqrt{(n+k_{UHF})\,\mathbf{P}_k + \mathbf{Q}_k}\right)_i & i = 1,\ 2,\ ...,\ n\\ \tilde{\mathbf{x}}_k - \left(\sqrt{(n+k_{UHF})\,\mathbf{P}_k + \mathbf{Q}_k}\right)_i & i = n+1,\ ...,\ 2n\end{cases} \tag{18}$$

where χ is a matrix consisting of (2n+1) vectors with $k_{UHF} = \alpha_{UHF}^2\,(n+\lambda_{UHF}) - n$, where k_{UHF} is a scaling parameter, and constant α_{UHF} determines the extension of these vectors around $\tilde{\mathbf{x}}_k$. We set α_{UHF} equal to 10^{-2} and λ_{UHF} is set equal to (3n). The sigma points are transformed or propagated through the nonlinear function, the so-called unscented transformation, to give:

$$\begin{aligned}\chi_{i,k+1} &= f(\chi_{i,k},\ \mathbf{u}_k)\\ \mathbf{Y}_i &= h(\chi_{i,k},\ \mathbf{v}_k)\end{aligned} \quad i = 0,\ 1,\ ,...,\ 2n \tag{19}$$

The mean value and covariance of y are approximated using the weighted mean and covariance of the transformed vectors[11)]

$$\begin{aligned}\hat{\mathbf{y}} &= \sum_{i=0}^{2n} W_i^{(m)}\mathbf{Y}_i\\ \mathbf{P}_y &= \sum_{i=0}^{2n} W_i^{(c)}\,(\mathbf{Y}_i - \hat{\mathbf{y}})\,(\mathbf{Y}_i - \hat{\mathbf{y}})^T\end{aligned} \tag{20}$$

where $W_i^{(m)}$ and $W_i^{(c)}$ are the weighted sample mean and covariance given by:

$$\begin{aligned}W_0^{(m)} &= k_{UHF}/(n+k_{UHF})\\ W_0^{(c)} &= k_{UHF}/(n+k_{UHF}) + (1-\alpha_{UHF}^2+\beta_{UHF})\\ W_i^{(m)} &= W_i^{(c)} = k_{UHF}/[2(n+k_{UHF})],\quad i = 1,\ 2,\ ...,\ 2n\end{aligned} \tag{21}$$

and β_{UHF} is used to incorporate prior knowledge of the distribution with $\beta_{UHF} = 2$.[12)] The predicted mean of the state vector $\tilde{\mathbf{x}}_k^-$, the covariance matrix $\tilde{\mathbf{P}}_k^-$, and the mean observation $\tilde{\mathbf{y}}_k^-$ can be approximated using the weighted mean and covariance of the transformed vectors:

$$\begin{aligned}\chi_{k|k-1}^i &= f\left(\chi_{k-1}^i,\ \mathbf{u}_k\right)\\ \tilde{\mathbf{x}}_k^- &= \sum_{i=0}^{2n} W_i^{(m)}\chi_{k|k-1}^i\\ \mathbf{P}_k^- &= \sum_{i=0}^{2n} W_i^{(c)}\left[\chi_{\mathbf{k|k-1}}^{\mathbf{i}} - \tilde{\mathbf{x}}_k^-\right]\left[\chi_{\mathbf{k|k-1}}^{\mathbf{i}} - \tilde{\mathbf{x}}_k^-\right]^T + \mathbf{Q}_k\\ \mathbf{Y}_{k|k-1}^i &= h\left(\chi_{k|k-1}^i\right)\\ \tilde{\mathbf{y}}_k^- &= \sum_{i=0}^{2n} W_i^{(m)}\mathbf{Y}_{k|k-1}^i\end{aligned} \tag{22}$$

The updated covariance $\mathbf{P}_{y,k}$ and the cross correlation matrix $\mathbf{P}_{xy,k}$ are:

$$\begin{aligned}\mathbf{P}_{y,k} &= \sum_{i=0}^{2n} W_i^{(c)}\left[\mathbf{Y}_{\mathbf{k|k-1}}^{\mathbf{i}} - \tilde{\mathbf{y}}_k^-\right]\left[\mathbf{Y}_{\mathbf{k|k-1}}^{\mathbf{i}} - \tilde{\mathbf{y}}_k^-\right]^T + \mathbf{R}_k\\ \mathbf{P}_k^- &= \sum_{i=0}^{2n} W_i^{(c)}\left[\chi_{\mathbf{k|k-1}}^{\mathbf{i}} - \tilde{\mathbf{x}}_k^-\right]\left[\mathbf{Y}_{\mathbf{k|k-1}}^{\mathbf{i}} - \tilde{\mathbf{y}}_k^-\right]^T\end{aligned} \tag{23}$$

Finally, the filter state vector $\tilde{\mathbf{x}}_k$ and covariance updated matrix $\mathbf{P}_{x,k}$ are represented as follows:

$$\begin{aligned}\tilde{\mathbf{x}}_k &= \tilde{\mathbf{x}}_k^- + \mathbf{K}\,(\mathbf{y}_k - \tilde{\mathbf{y}}_k)\\ \left(\mathbf{P}_k^+\right)^{-1} &= \left(\mathbf{P}_k^-\right)^{-1} + \left(\mathbf{P}_k^-\right)^{-1}\mathbf{P}_{xy,k}\mathbf{R}_k^{-1}\left[\left(\mathbf{P}_k^-\right)^{-1}\mathbf{P}_{xy,k}\right]^T - \vartheta_k\mathbf{I}_d\\ \mathbf{K} &= \mathbf{P}_{xy,k}\mathbf{P}_{y,k}^{-1}\end{aligned} \tag{24}$$

where $\mathbf{K}$ is the Kalman gain matrix, ϑ_k is the performance bound of the H_∞ filter, and R_k is a suitable matrix which, in the case of a normal distribution, coincides with the measurement noise covariance matrix at time step k. In order to assure that the covariance matrix is positive definite this value is calculated at each iteration as:

$$\vartheta_k^{-1} = \xi max\left(eig\left(\left(\mathbf{P}_k^-\right)^{-1} + \left(\mathbf{P}_k^-\right)^{-1}\mathbf{P}_{xy,k}\mathbf{R}_k^{-1}\left[\left(\mathbf{P}_k^-\right)^{-1}\mathbf{P}_{xy,k}\right]^T\right)^{-1}\right) \tag{25}$$

As one can see from the set of equations (24), the performance bound has no direct effect on the calculation of the gain and on the update step for the estimated state. Nonetheless ϑ_k modifies the shape of covariance matrix update, which, in turn, generates a different distribution of the sigma points. In this way, the propagation and the update step at the following time step will be directly influenced by the value of the performance bound.

5.1. Filtering with Chebyshev Polynomial Algebra

The use of an unscented transformation to calculate the propagated covariance matrix was shown to be a good solution to recover some nonlinearities in the dynamics. On the other hand, the Unscented Transformation starts from the strong assumption of symmetric Gaussian distribution and provides anyway a second order approximation to the distribution of the propagated states.

In order to better capture the nonlinearities in the dynamics, in this paper, we propose the use of a recently developed polynomial algebra based on Chebyshev polynomial expansions.

The function space $\mathcal{P}_{n,d}(\alpha) =< \alpha_{\mathbf{I}}(\mathbf{b}) >$ where $\mathbf{b} \in \Omega \subset \mathbb{R}^d$, $\mathbf{I} = (i_1, \ldots, i_d) \in \mathbb{N}_+^d$ and $|\mathbf{I}| = \sum_{j=1}^d i_j \leq n$, is the space of polynomials in the α basis up to degree n in d variables. This space can be equipped with a set of elementary arithmetic operations, generating an algebra on the space of polynomials such that, given two elements $A(\mathbf{b})$, $B(\mathbf{b}) \in \mathcal{P}_{n,d}(\alpha)$ approximating any two real multivariate functions $f_A(\mathbf{b})$ and $f_B(\mathbf{b})$, it stands that

$$f_A(\mathbf{b}) \oplus f_B(\mathbf{b}) \sim A(\mathbf{b}) \otimes B(\mathbf{b}), \tag{26}$$

where $\oplus \in \{+, -, \cdot, /\}$ and $\otimes$ is the corresponding operation in $\mathcal{P}_{n,d}(\alpha_i)$. This allows one to define the algebra $(\mathcal{P}_{n,d}(\alpha_i), \otimes)$, of dimension $\dim(\mathcal{P}_{n,d}(\alpha_i), \otimes) = \mathcal{N}_{d,n} = \binom{n+d}{d}$, the elements of which belong to the polynomial ring in d indeterminates $\mathbb{R}[\mathbf{b}]$ and have degree up to n. Each element $P(\mathbf{b})$ of the algebra, is uniquely identified by the set of its coefficients $\mathbf{p} \in \mathbb{R}^{\mathcal{N}_{d,n}}$ such that

$$P(\mathbf{b}) = \sum_{\mathbf{I},|\mathbf{I}|\leq n} p_{\mathbf{I}}\alpha_{\mathbf{I}}(\mathbf{b}). \tag{27}$$

In the same way as for arithmetic operations, it is possible to define a composition rule in the polynomial algebra and hence the counterpart, in the algebra, of the elementary functions $\{\sin(y), \cos(y), \exp(y), \log(y), ...\}$. Differentiation and integration operators can also be defined. By defining the initial conditions and model parameters of the dynamics as element of the algebra and by applying any integration scheme with operations defined in the algebra, at each integration step is available the polynomial representation of the state flow. The main advantage of the method is in the control of the trade-off between computational complexity and representation accuracy at each step of integration. Furthermore, sampling and propagation are decoupled, therefore, irregular regions can be propagated with a single integration, provided that a polynomial expression is available. It has been shown that the polynomial algebra approach presents overall good performance and scalability (with respect to the size of the algebra) compared to its non-intrusive counterpart. On the other hand, being an intrusive method, it cannot treat the dynamics as black box. Its implementation requires operator overloading for all the algebraic operations and elementary functions defining the dynamics, making it more difficult to implement than a non-intrusive method.

The algebra is used to propagate the set of variated states in place of the Unscented Transformation. The idea is to replace the numerically integrated states:

$$\mathbf{X}_{k+1,i} = \mathbf{f}(\mathbf{X}_{k,i}, \mathbf{u}_{k,i}), \tag{28}$$

where $\mathbf{f}$ is the integration of the dynamics from state k to state $k+1$ at sample i, with the full polynomial representation of the set of final states:

$$\mathbf{X}_{k+1,i} = \mathbf{P}(\mathbf{X}_{k,i}, \mathbf{u}_{k,i}), \tag{29}$$

where the polynomials $\mathbf{P}$ are defined as in Eq.(27). The rest of the filter remains unchanged.

5.2. Multi-spacecraft Data Fusion Process

Having defined the filtering and control processes, each spacecraft needs to data fuse its own measurements and the information shared with the other spacecraft. This section describes the data fusion process implemented to address this issue. Each spacecraft receives the whole set of measurements coming from all the members and builds the necessary matrices for the filtering process. The analysis in this paper is limited to the case in which inter-spacecraft measurements are synchronous with a single common time tag. In the case of asynchronous measurements a different time tag is associated to each measurement.

The information sharing and fusion is achieved by exploiting the inter-spacecraft measurement of equation (13). In fact, when a new inter-spacecraft measurement is available for spacecraft i, spacecraft j transmits back the current estimation of its own state to be used in the estimation process. This is necessary because the position of spacecraft j is required in order to compute the predicted relative distance measurements.

The estimation process, for each spacecraft, can be described through the following 3 main steps:

1. At initial time t_0, each spacecraft initialises its filter with the initial guesses on the state, $\mathbf{X_0}$, and covariance, $\mathbf{P_0}$ The sigma points, relative to all the sensors mounted on the spacecraft, are generated according to the UHF implementation algorithm;
2. The estimated state and the sigma points are propagated from t_k to t_{k+1};
3. At time t_{k+1}, predicted and actual measurements are available. In case of inter-spacecraft measurements, each spacecraft transmits its current state, according to its

knowledge. If the number of measurements is lower than the predicted number, only the consistent measurements between the two steps are considered in the update step. This is obtained by removing the predicted measurements and the correspondent columns and rows in the filter gain.

6. Results

The binary asteroid system chosen as environment for the simulations is 65803 Didymos, whose parameters are listed in Table 1. For simplicity reasons, the orbital motion of the system around the Sun has been considered circular and laying in the ecliptic. The dimensions and gravitational parameters are chosen according to the current knowledge of the system. The secondary body is tidal locked. The cameras are assumed to

Semi-major axis	a	1.6446 AU
Eccentricity	e	0.3838
Inclination	i	3.4077 deg
RAAN	Ω	73.2219 deg
Argument of periapsis	ω	319.2516 deg
Orbital period	T_D	2.11 yr
Distance AB	d_{AB}	1.18 km
System rot. period	T_{AB}	11.92 h
Grav. param. A	μ_A	$3.4908 * 10^{-8} km^3/s^2$
Physical dimensions	a_A, b_A, c_A	387.5, 387.5, 387.5 m
Rotational velocity	ω_A	2.26 h
Grav. param. B	μ_B	$3.1781 * 10^{-10} km^3/s^2$
Physical dimensions	a_B, b_B, c_B	81.5, 62.7, 52.2 m
Rotational velocity	ω_B	11.92 h

Table 1. Orbital and physical parameters for 65803 Didymos

have a resolution of 300x300 pixels, with a field of view of 50 degrees. Table 2 summarizes the measurement errors used in the simulations. The LIDAR range error is set to 10 m according to Kubota et al. (2003), and a precision of 2 m is used for the inter-spacecraft LIDAR range measurement error. Angular measurements and attitude errors are from Yim et al. (2000). It is assumed that the measurements from Earth are taken from an ideal ground station positioned at (0.0 deg latitude and 0.0 deg longitude) with minimum served elevation of 0.0 deg. The mass of each spacecraft is constant and equal to 500 kg, the maximum cross section area is 20 m^2 and reflectivity coefficient C_R is assumed equal to 2. The initial estimated state is always equal to the real initial state augmented by some bias. Specifically, the position components are always increased by 100m and the velocity ones by 1m/s. The initial covariance matrix is a diagonal matrix whose elements are equal to the square of twice the initial error for each component of the state. As a final remark, for all the test cases the application of the control is delayed by 2 hours, in order to allow the filters to converge. In both the scenarios presented the spacecraft will be required to keep a stable trajectory close to the Lagrangian point L4 of the binary system. This point, due to the irregularities in the gravitational field of the system and the presence of the Sun (gravitational perturbation and radiation pressure) is unstable and the spacecraft is soon swept away if no control is applied.

Sensors errors $1-\sigma$		
Camera pixelisation	$\zeta_{\varphi,\psi}$	$10^{-3} rad$
LIDAR	ζ_l	$10\ m$
Inter-sat distance	$\zeta_{d_{rel}}$	$2\ m$
Inter-sat angles	$\zeta_{\varphi_{rel},\psi_{rel}}$	$10^{-3} rad$
GS range	$\zeta_{\rho_{GS}}$	$20\ m$
GS angles	$\zeta_{\varphi_{GS},\psi_{GS}}$	$5.5\ 10^{-3} deg$

Table 2. Sensors errors

6.1. Case 1: single spacecraft with ground station link

In this scenario, the satellite is positioned at the Lagrangian point L4 and the initial conditions are such that the ground station sees the spacecraft at the zenith. Figure 4 shows the trajectory of the spacecraft around the Lagrangian point in the reference frame rotating with the binary system. In the first two hours, before the control law takes over, the spacecraft starts drifting away from the Lagrangian point in direction top-left. When the spacecraft reaches the furthermost point from the initial position, the control starts acting and the spacecraft is pushed in proximity of L4. A blue marker indicates the final position of the spacecraft at the end of the simulation. The oscillatory noisy motion of the spacecraft around the Lagrangian point is due to the nature of the control law and the uncertainty in the estimation of its state. Figure 5 reports the error in the estimation of the position of the spacecraft. It can be seen that, after a short transient, the estimation converges to a value of 6.96 m. Such a value for the position error is of the same order

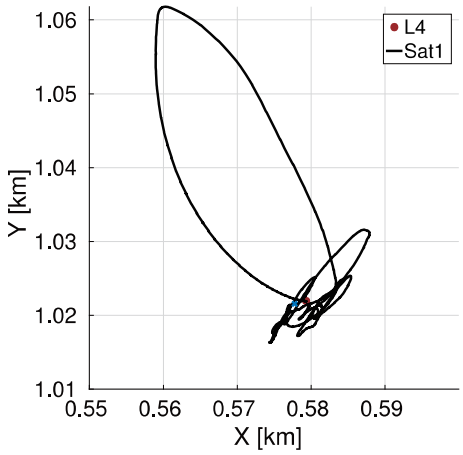

Fig. 4. Case 1: trajectory of the spacecraft around L4

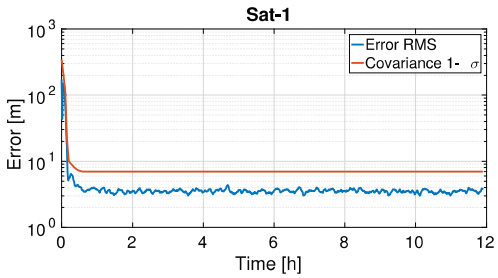

Fig. 5. Case 1: position error

of magnitude expected from the uncertainty on the measurements of the Camera/LIDAR combination. It can be seen, then, that the use of such a sensor, together with appropriate tuning of the weighting coefficients in the information from the measurements, is capable of compensating the much higher error induced by the measurements from the ground station.

6.2. Case 2: formation of 4 spacecraft

In this scenario, a formation of 4 spacecraft is positioned around the Lagrangian point L4. The initial conditions are such that all the spacecraft has the same y coordinate of L4 but a bias one the x component. These biases are +10m for Sat-1, +20m for Sat-2, -10m for Sat-3 and -20m for Sat-4. Figure 6 shows the evolution of the trajectories, while Figures 7 to 10 show the error in the estimation of the position for all the 4 spacecraft.

The results obtained are very similar to the ones shown in the previous case. This is a proof that the set of measurements used, LIDAR, camera and inter-satellite link, is capable of making the formation navigate autonomously without the need of any Earth-based information. The evolution of the trajectories in Figure 6 shows that all the spacecraft have a wider oscillation in one direction (bottom left to top right). Such direction is the one that leads to the primary asteroid, the one used for the measurements. This agrees with the values of the error components of the LIDAR/camera measurements, since the uncertainty on the distance is greater that the transverse one due to the uncertainty on the pointing angles. The average computational time for these simulations was of 85.8168 seconds.

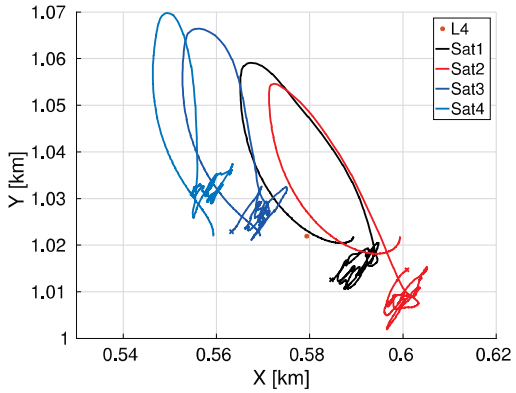

Fig. 6. Case 2: trajectories of the 4 spacecraft in proximity of L4

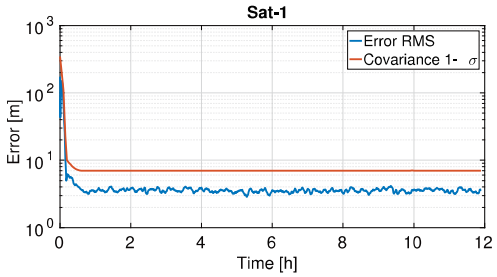

Fig. 7. Case 2: position error for Sat-1

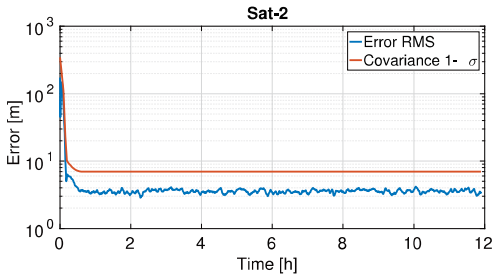

Fig. 8. Case 2: position error for Sat-2

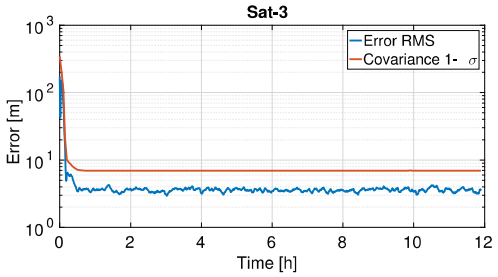

Fig. 9. Case 2: position error for Sat-3

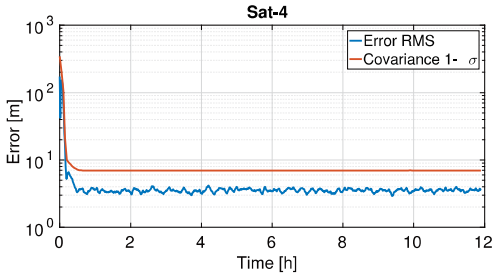

Fig. 10. Case 2: position error for Sat-4

6.3. Case 3: formation of 4 spacecraft with Chebyshev algebra propagation

In this test case, the use of the Chebyshev algebra, described in Section **5.1.**, is employed in the estimation process. The polynomial representation is carried on by the use of third order polynomials in the 6 variables of the dynamical state. Before each propagation, from time t_k to time t_{k+1}, upper and lower boundaries to the polynomial space are set according to the current uncertainty. After the propagation, the new sigma points are sampled and used for the usual estimation process. The scenario shown is the same of the previous section (**6.3.**). Figure 11 shows the trajectories of the 4 spacecraft, while Figure 12 to 15 show the position estimation errors for the four spacecraft. The comparison of these results with the ones of the previous test case shows the perfect agreement in the state estimation for all the spacecraft. The average computational time for this test case was 85.7269 seconds. This implies that the use of the algebra requires the same computational resources of the Unscented Transformation in this particular case. Note that, in this paper, the use of the algebra is limited to the propagation of the dynamics but the filter still uses only the first two statistical moments. However, the information carried by the propagation of the uncertainty with the algebra would allow the use of a complete description of the probability distribution and, therefore, would allow one to drop any hypothesis on the Gaussian nature of the noise. An UHF based on the simple propagation of the dynamics of the algebra has to be taken as a first illustrative example but does not fully exploit the potentiality of this approach.

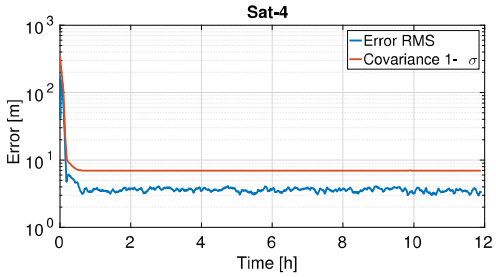

Fig. 15. Case 3: position error for Sat-4

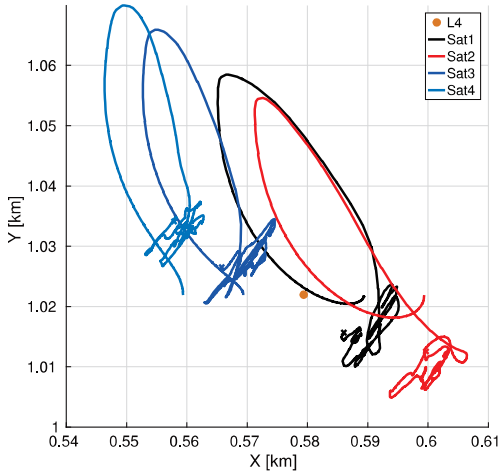

Fig. 11. Case 3: trajectories of the 4 spacecraft in proximity of L4

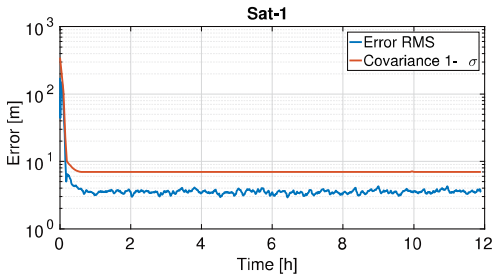

Fig. 12. Case 3: position error for Sat-1

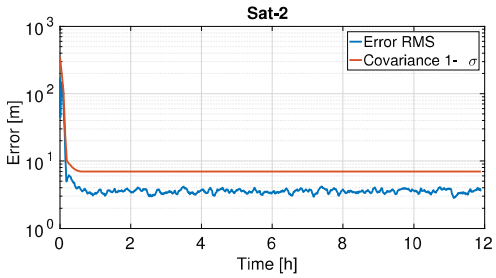

Fig. 13. Case 3: position error for Sat-2

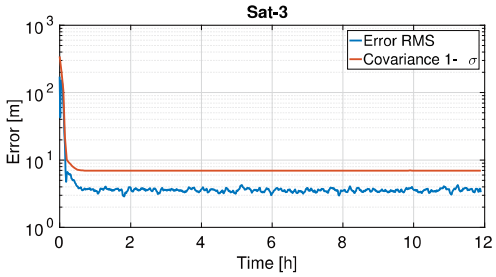

Fig. 14. Case 3: position error for Sat-3

7. Conclusion

The paper presented some first results on the autonomous navigation of a formation of spacecraft in the proximity of a binary system. The formation was specifically trying to maintain the position of the spacecraft around L4. It was demonstrated that with a combination of optical measurements and inter-spacecraft links the formation could be controlled within an error of few meters. The next step will be to test delays and failures in the sensors and the communication chain as previous done for the case of a single asteroid. The paper introduced also the use of a generalised polynomial algebra based on Chebyshev polynomials for the propagation of the dynamics. In future work the potentiality of the algebra will be extended to the propagation of the full probability distribution rather than limiting the construction of the filter only on the first two statistical moments.

References

1) Vetrisano M., Vasile M. Autonomous Navigation of a Spacecraft Formation in the Proximity of an Asteroid. Advances in Space Research, Volume 57, Issue 8, 15 April 2016, Pages 17831804
2) Vetrisano M., Vasile M., Colombo C., Asteroid Rotation and Orbit Control via Laser Ablation. Advances in Space Research, Volume 57, Issue 8, 15 April 2016, Pages 17621782.
3) Thiry, N. and Vasile, M., Binary Asteroid Manipulation with Laser Ablation. HPLA/DE, Santa Fe, 4-6 April 2016.
4) Riccardi, A., Tardioli, C., Vasile, M., An Intrusive Approach to Uncertainty Propagation in Orbital Mechanics Based on Tchebycheff Polynomial Algebra. Astrodynamics Specialists Conference, AAS 15-544, Veil, Colorado, USA, 9-13 August 2015
5) Scheeres, D.J. Orbit Mechanics about Asteroids and Comets. Journal of Guidance, Control and Dynamics, 2012, 35(3): 987-997.
6) Hu, W. and Scheeres, D.J. Spacecraft motion about slowly rotating asteroids. Journal of Guidance, Control and Dynamics 25 (4), JulyAugust 2002, 765775.
7) Li, S., Cui, P.Y., Cui, H.T. Vision-aided inertial navigation for pinpoint planetary landing. Aerospace Science and Technology, 2007, 11(6):499-506.
8) Kubotaa, T., Hashimotoa, T., Sawai, S., Kawaguchib, J., Ninomiyaa, K., Uoc, M., Babac, K. An autonomous navigation and guidance system for MUSES-C asteroid landing. Acta Astronautica 52 (2003) 125 131.
9) Dionne, K. Improving Autonomous Optical Navigation for Small Body Exploration Using Range Measurements. AIAA 2009-6106. AIAA Guidance, Navigation, and Control Conference, 10 - 13 August 2009, Chicago, Illinois.
10) Alonso, R., Du, J., and Hughes, Y Relative Navigation for Formation Flying of Spacecraft. Proceedings of the Flight Mechanics Symposium, NASA-Goddard Space Flight Center, Greenbelt, MD, 2001, pp. 115-129.
11) Julier, J. K. Uhlmann and Durrant-Whyte, H.F. A new approach for filtering nonlinear systems, Proceedings of the American Control conference, Seattle, Washington, 1995.
12) Crassidis, J.L., and Junkins, J.L. Optimal Estimation of Dynamic Systems, 1st Edition, Chapman Hall/CRC Press, Boca Raton, FL, 2004.